

Orbits through polytropes

Amalia Gjerløv, and W. Dean Pesnell

Citation: American Journal of Physics **87**, 452 (2019); doi: 10.1119/1.5093295

View online: <https://doi.org/10.1119/1.5093295>

View Table of Contents: <https://aapt.scitation.org/toc/ajp/87/6>

Published by the American Association of Physics Teachers

ARTICLES YOU MAY BE INTERESTED IN

The sliding ladder problem revisited in phase space

American Journal of Physics **87**, 444 (2019); <https://doi.org/10.1119/1.5096278>

Gravity-driven fluid oscillations in a drinking straw

American Journal of Physics **87**, 433 (2019); <https://doi.org/10.1119/1.5095945>

Electromagnetic surface wave propagation in a metallic wire and the Lambert W function

American Journal of Physics **87**, 476 (2019); <https://doi.org/10.1119/1.5100943>

Gravitational waves from orbiting binaries without general relativity

American Journal of Physics **86**, 186 (2018); <https://doi.org/10.1119/1.5020984>

Lagrangian vs Hamiltonian: The best approach to relativistic orbits

American Journal of Physics **86**, 678 (2018); <https://doi.org/10.1119/1.5047439>

The candle seesaw

American Journal of Physics **87**, 370 (2019); <https://doi.org/10.1119/1.5096886>



Orbits through polytropes

Amalia Gjerløv and W. Dean Pesnell^(a)

NASA, Goddard Space Flight Center, Greenbelt, Maryland 20771

(Received 5 April 2017; accepted 16 February 2019)

We describe how orbital tunnels could be used to transport payloads through the Earth. If you use a brachistochrone for the tunnel, the body forces in the tunnel become overwhelmingly large for small angular distances traveled. Projectiles move along an orbital tunnel faster than they would along a brachistochrone connecting the same points but the body force components cancel. We describe how parabolic Keplerian orbits outside the object merge onto quasi-Keplerian orbits inside the object. We use models of the interior of the Earth with three values of the polytropic index (n) to calculate interior orbits that travel between surface points. The $n=3$ results are also scaled to the Sun. Numerical integrations of the equations describing polytropes were used to generate the initial models. Numerical integration of the equations of motion are then used to calculate the angular distance you can travel along the surface and the traversal time as a function of the parabolic periapsis distance for each model. Trajectories through objects of low central condensation show a focussing effect that decreases as the central condensation increases. Analytic solutions for the trajectories in a homogeneous sphere are derived and compared to the numeric results. The results can be scaled to other planets, stars, or even globular clusters. © 2019 American Association of Physics Teachers.

<https://doi.org/10.1119/1.5093295>

I. INTRODUCTION

What would be the best route to build a tunnel through the Earth to transport people and cargo from one place to another? Chord tunnels are straight lines between surface points that use the Earth's gravity to accelerate the projectile to a high speed during the first half of the trip and the same force to reduce the speed back to rest during the second half. They have the same travel time for all separation distances.¹ A chord tunnel was imagined as a "burrito delivery service" between California and New York.² The tunnel problem can be generalized to brachistochrones connecting points on the surface of the Earth.³ A brachistochrone is the path along which it takes the least amount of time for a projectile to travel from one end to the other assuming an initial velocity of zero. Orbital tunnels, which are introduced here, are another possible path through a planet or star. They assume the projectile follows a quasi-Keplerian orbit through the object with a trajectory described by the mathematics of orbital motion. These tunnels compete against surface transportation solutions such as SpaceX's Hyperloop⁴ that use above-grade vacuum tubes to permit high-speed trains.

As soon as you start examining motions through a mass distribution you must allow for the change in mass density with radial distance in the object's interior. The simplest model of interior of the Earth is a homogeneous sphere that has a constant density profile with radius. This model has the advantage that closed forms of solutions exist for many problems. Figure 1 illustrates four possible paths through a homogeneous sphere: a straight-line chord, brachistochrone, parabolic Keplerian orbit, and a quasi-Keplerian orbit that we define below, all traversing an angular distance of 120° at the surface. Each trajectory in this figure can be written in a closed form. This also illustrates the reason to consider orbits—the body forces are much smaller for the orbits. The centrifugal and gravitational accelerations for the chord and brachistochrone tunnels are in the same direction and can add to intolerable levels. Because the initial velocities are

much higher, the traversal times are shorter for the orbits than for the chord and brachistochrone tunnels.

Other models of the mass distribution should also be examined, especially given that the gravity inside a homogeneous sphere decreases from the surface inward. That unrealistic variation induces the same-travel-time property of chord tunnels. Travel tunnels can also be calculated through more complicated models of the Earth. The fall-through times and brachistochrones have been calculated for the Preliminary Reference Earth Model (PREM)⁵ and for planetary models where the mass density varied as a power law of the radius.⁶

Polytropes provided the mass density profiles needed to calculate the fall-through times and brachistochrone traversal times as a function of central condensation (the ratio of the central to average density) and tangent radius.⁷ The travel times for brachistochrones connecting two surface points with different tangent radii were listed for the PREM, several polytropes, and a set of completely degenerate objects. For a given tangent radius the angular distance traversed by a brachistochrone decreases as the central condensation increases. The main conclusion was that as the central condensation increases the brachistochrones must reach deeper depths to travel the same angular distance at the surface of the object. Because this effect is related to the location of the peak of the gravity inside the object, this effect is apparent at even small changes from the homogeneous sphere, such as when the PREM is used.⁵

Because a brachistochrone is convex with respect to the center of the Earth, the acceleration of gravity and centrifugal acceleration act in concert on the projectile, while the normal force from the walls of the tunnel must act in opposition to keep the train in the tunnel. As we show below, these forces can be quite large for brachistochrone tunnels in the Earth and enormous for orbits passing through the Sun or other star.

But another option exists—tunnels shaped to follow an orbital trajectory. Unlike the chord and brachistochrone tunnels, Orbital tunnels are concave with respect to the center,

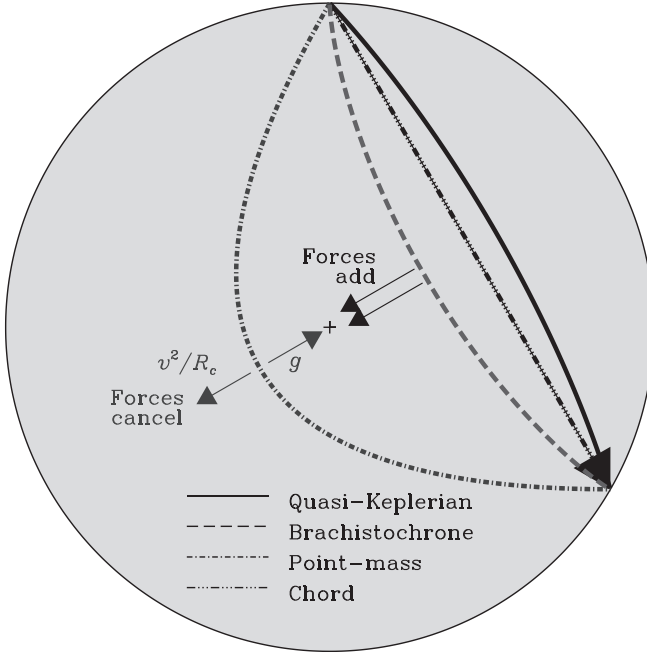


Fig. 1. Four tunnels through a homogeneous sphere scaled to the Earth that span an angular distance of 120° . The long chain-dashed arrow is a chord tunnel from the pole to the point 120° away that takes about 42 min to traverse (Ref. 1). The dashed curve is a brachistochrone between the same points, which requires 39 min for the trip (Ref. 3). The solid curve is a quasi-Keplerian orbit (described below) that moves under the changing gravitational acceleration inside the sphere and requires 16 min to traverse the 120° separation. The dotted-dashed curve is a Keplerian parabola orbit (that does not account for the change in mass along the orbit) with a perihelion distance of 0.25, which requires 16.5 min to move from one surface point to the other. While a projectile moving along the first two curves begins its flight from rest, it must be accelerated to 11.2 km/s at the surface to use the other two orbits. Another difference is the angle of incidence. The brachistochrone starts from a vertical position, while the parabola, quasi-Keplerian orbit, and chord begin at a slope of 60° . Two short arrows show the direction of the gravitational and centrifugal accelerations for the Keplerian parabola and notes that they cancel. The other short black arrows illustrate how both forces act in the same direction for the brachistochrone.

so the gravitational and centrifugal accelerations act in opposition and no body forces are required to maintain the trajectory. However, a large initial velocity is necessary to enter the trajectory at the surface.

Examples of orbits of objects through spherical mass distributions are found throughout physics. Stars orbiting in the spherical star associations called globular clusters move quickly through periapsis and spend most of their time far from the core. Each periapsis passage causes the line of apsides to rotate and generate petal orbits.⁸ Weakly interacting massive particles (WIMPs) have been postulated as one way to solve the dark matter problem. WIMPs moving through the Milky Way could be caught by the Sun and form a halo.^{9,10} Quarks move in a potential energy that is often assumed to be a simple harmonic oscillator, which corresponds to the homogeneous sphere. Another example is the excitation of p -modes as a primordial black hole passes through the Sun.¹¹ Trajectories in all of these systems can be studied with the techniques developed here.

The research described here extends the work of Pesnell⁷ to using orbital tunnels to travel from one surface point to another. We will call such orbital tunnels quasi-Keplerian orbits to distinguish them from the well-studied Keplerian orbits where a satellite moves in the $1/r$

gravitational potential of a point mass. First, we will describe the properties of the polytropes used here. We then show that the body accelerations of objects traveling along brachistochrones are too large for these trajectories to be used for transport. Quasi-Keplerian orbits are then introduced and calculated for two central objects, three polytropic indices, and a set of periapsis distances for the incoming parabolic Keplerian orbits used as initial conditions. We will also show that the change in angular distance at the surface and traversal time have analytic solutions for homogeneous spheres. All of these calculations identify the polytropic function as the gravitational potential to simplify the solutions.

II. POLYTROPES

Conditions deep inside planets and stars have not been directly measured. But they can be estimated from models that satisfy the conservation equations from the center to the surface and use the measured global quantities, such as mass and radius, as boundary conditions. The homogeneous sphere, which has a constant density throughout the model, is also a member of the polytrope family of models.

Polytropes are models of stars and planets that use the equation of state $P = K\rho^{1+1/n}$ to derive hydrostatic configurations of the pressure (P) and mass density (ρ). The polytropic equation of state (EOS) relates P to ρ with a constant K and the polytropic index n . While the value of n is a critical parameter in our discussion, the value of K is usually not specified in a polytrope. Instead, the values of the central pressure (P_c) and density (ρ_c) will be determined by the mass of the object (M_*) and its radius (R_*). The $n=0$ polytrope corresponds to the homogeneous sphere and $n \rightarrow 5$ is the limit of the family of solutions discussed here. Because they have a peak in the gravitational acceleration inside the object, polytropes with $n > 0$ provide a more accurate variation of gravity with radius for calculating internal trajectories than does a homogeneous sphere.

Following the derivation in Chapter 4 of Ref. 12, the equation of spherical hydrostatic equilibrium

$$\frac{1}{\rho} \frac{dP}{dr} = -\frac{GM(r)}{r^2}, \quad (1)$$

which represents the balance of the pressure gradient and gravitational acceleration, is combined with the equation of mass conservation

$$\frac{dM(r)}{dr} = 4\pi r^2 \rho, \quad (2)$$

to yield a Poisson equation that links the run of pressure and mass density within the model

$$\frac{1}{r^2} \frac{d}{dr} \left(\frac{r^2 dP}{\rho dr} \right) = -4\pi G\rho. \quad (3)$$

The polytropic EOS provides another relationship between P and ρ . The polytropic function θ is introduced as $\rho = \rho_c \theta^n$, where ρ_c is the mass density at the center of the model, and a new independent variable ξ , which is defined by $r = \epsilon \xi$, where

$$\varepsilon^2 = \frac{(n+1)K}{4\pi G} \rho_c^{1/n-1}, \quad (4)$$

is found by gathering the scaling factors of the quantities in Eq. (4). The result is the Lane-Emden equation

$$\frac{1}{\xi^2} \frac{d}{d\xi} \left(\xi^2 \frac{d\theta}{d\xi} \right) = -\theta^n. \quad (5)$$

A solution of Eq. (5) requires two boundary conditions, which are chosen to be $\theta=1$ and $d\theta/d\xi=0$ at the center of the model, $\xi=0$. The surface of the model (ξ_0) is at the first zero of θ , so $R_* = \varepsilon \xi_0$. The properties of the solutions to Eq. (5) are discussed in Chapter 4 of Ref. 12. Physical solutions for θ exist for $0 \leq n < 5$, where $n=0$ corresponds to the homogeneous sphere (the density is constant while the pressure is $P(\xi) = P_c[1 - \xi^2/\xi_0^2]$) and $n=5$ corresponds to an object with an infinite size but finite central density and mass.

One useful relationship for a polytrope is the mass within a sphere of radius ξ

$$M(\xi) = -4\pi\rho_c\varepsilon^3 \xi^2 \frac{d\theta}{d\xi}, \quad (6)$$

which, when evaluated at the surface, gives the mass of the polytrope

$$M_* = -4\pi\rho_c\varepsilon^3 \xi_0^2 \frac{d\theta}{d\xi} \Big|_{\xi_0} = \frac{4\pi}{3} \bar{\rho} R_*^3. \quad (7)$$

This definition of M_* can be manipulated to give the central condensation of a model, the ratio of the central density to the mean density, as

$$\frac{\rho_c}{\bar{\rho}} = -\frac{\xi_0}{3} \left(\frac{d\theta}{d\xi} \Big|_0 \right)^{-1} \equiv -\frac{\xi_0}{3} (\theta'_0)^{-1} \quad (8)$$

evaluated at ξ_0 .

All properties of a polytrope matched to an object are specified by the mass and radius of the object. For example, the central pressure of a star is given by

$$\begin{aligned} P_c &= \frac{1}{4\pi(n+1)(\theta'_0)^2} \frac{GM_*^2}{R_*^4} \\ &= \frac{8.975 \times 10^{14}}{(n+1)(\theta'_0)^2} \frac{(M_*/M_\odot)^2}{(R_*/R_\odot)^4} \text{ dyne cm}^2, \end{aligned} \quad (9)$$

where $M_\odot = 1.9891 \times 10^{33}$ g is the mass of the Sun and $R_\odot = 6.955 \times 10^{10}$ cm is the radius of the Sun. This means that the value of K is not needed to describe the polytrope.

The radial gravitational acceleration also can be derived from Eq. (6)

$$g = \frac{GM(r)}{r^2} = -4\pi G \rho_c \varepsilon \frac{d\theta}{d\xi}. \quad (10)$$

Integrating Eq. (10) with radius gives the spherically symmetric gravitational potential for motion completely contained inside a polytrope:

$$\Phi_{in} = -4\pi G \rho_c \varepsilon^2 \theta. \quad (11)$$

III. PROPERTIES OF ANALYZED POLYTROPS

Polytrope models for $n=0, 1$, and 3 were integrated with the Runge-Kutta shooting method described by Pesnell.^{7,13,14} A value is chosen for ξ_0 and the Lane-Emden equation [Eq. (5)] is integrated from $\xi=0$ towards the surface until θ changes sign. A Newton's method is then used to converge the value of ξ_0 . Values for ξ_0 , $\rho_c/\bar{\rho}$, $-\xi_0^2\theta'_0$, the fall-through time (T_f), and the maximum velocity (v_{max}) of a projectile freely falling through the center of an Earth-matched polytropic model for each n are listed in Table I. The variation of ρ/ρ_c and g/g_{max} with normalized radius for several values of n are shown in Fig. 1 of Ref. 7. As n increases from 0 to 5 the model becomes more centrally condensed and the location of the maximum in the gravity moves inward.

The polytrope that best reproduces the central condensation of the PREM has $n=0.715$, but it matches neither the fall-through time nor the maximum velocity. We chose to work with the $n=1$ polytrope, which has the solution $\theta = \sin \xi/\xi$, as the intermediate model. The Sun is well represented by an $n=3$ polytrope, which has been called the Standard model. Only the $n=3$ polytrope needed to be numerically integrated for this research.

IV. BRACHISTOCHRONES AND THE STAPP SURVIVAL LIMIT

There are several reasons to move beyond the chords and brachistochrones previously considered as planetary tunnels. One is the magnitude of the body forces that act upon the projectiles and any passengers. Another is the time it takes to move through the tunnel. The travel time may be a minimum for the brachistochrones, but they assume the projectile starts from rest. Finally, the construction of chord and brachistochrone tunnels means moving deep into the Earth for modest angular separations at the surface. The quasi-Keplerian orbits are concave with respect to the center of the object and will always be closer to the surface than the other two types of tunnels.

We first summarize the limits of the magnitude of the acceleration that could be experienced by a human passenger. We then calculate the body accelerations along brachistochrones for polytropes scaled to the Earth and Sun. For ease of comparison, the brachistochrones will have the tangent radii listed in Table II of Ref. 7.

A. The Stapp survival limit

Any transportation system must neither injure its passengers nor harm its cargo. The body acceleration of passengers riding trains through the Earth should be examined as a limit to the tunnels' usefulness as a passenger service. One study showed that accelerations as low as 6 g's can either injure

Table I. Properties of earth-scaled polytropes.

n	ξ_0	$\rho_c/\bar{\rho}$	$-\xi_0^2\theta'_0$	T_f (min)	v_{max} (km/s)
0	2.449	1.00	4.899	42.20	7.91
PREM	—	2.36	—	38.13	8
0.715	2.908	2.36	3.473	36.96	10.2
1	3.142	3.29	3.142	35.64	11.2
3	6.896	54.2	2.018	31.13	20.7

humans or prevent them from functioning at their normal levels.¹⁵ This may explain why the maximum acceleration on roller coasters is reported to be near 6 g's.¹⁶ Seats in small airplanes must be able to protect a passenger to 26 g's during a crash.¹⁷

But these are not the highest accelerations that humans have survived. Between 1947 and 1954, Dr. John Paul Stapp endured many rides on rocket sleds to study what accelerations could be survived by humans. His 29th test showed that a human could survive 46.2 g's if properly harnessed.¹⁸ These tests caused the United States Air Force to increase the strengths of fighter jet cockpits and also showed that using seat belts would improve the survival rate of automobile crashes. To provide a marker, we have called 46.2 g's the Stapp Survival Limit and note that any conveyance that causes accelerations to seated passengers above that limit is an impractical means of transportation. Indeed, any transportation system with an acceleration that exceeds 6 g's for more than a brief period of time should be marked as hazardous to humans.

Cargo transport may allow higher accelerations. Satellites are subjected to large accelerations during launch and re-entry. For example, NASA currently requires vibrational testing of satellite components over a wide frequency range with a total RMS amplitude of 6.8 g's,¹⁹ although some frequency ranges are tested to higher amplitudes. One possible way to accelerate payloads to very high velocities are electromagnetic railguns that can produce accelerations of up to 20×10^3 g's (Ref. 20) and are anticipated to reach 40×10^3 g's.²¹ The compressive strength of materials then becomes the limiting factor to achieving orbital velocities.

B. Calculation of body forces

While brachistochrone tunnels through polytropes have been described,⁷ the body forces on objects traveling through them were not calculated. The forces have been mentioned for the homogeneous sphere but not evaluated.^{3,22} As an object falls through a polytrope in a frictionless, vacuum tunnel, the only body force that must be considered is the normal force exerted by the wall to keep the object in the tunnel. The acceleration due to this force depends on the local acceleration of gravity and the centrifugal acceleration caused by the curvature of the tunnel, or

$$a_N = \mathbf{g} \cdot \hat{\mathbf{N}} - v^2 |\boldsymbol{\kappa}|, \quad (12)$$

where v is the velocity of the payload, $\hat{\mathbf{N}}$ is the unit normal vector that points in the normal direction of the curve, $\mathbf{g} = -g \hat{\mathbf{r}}$ (where g comes from Eq. (10) and $\hat{\mathbf{r}}$ is the unit vector in the outward radial direction), $|\boldsymbol{\kappa}| \equiv \kappa$ is the reciprocal of the radius of curvature, and v^2 will be described below. As illustrated in Fig. 1, these accelerations add for the brachistochrone tunnel.

C. Body forces along a brachistochrone through a polytrope

Each term in Eq. (12) must be evaluated inside a polytrope. The normal unit vector in spherical polar coordinates is

$$\hat{\mathbf{N}} = \frac{1}{|\dot{\mathbf{r}}|} \left(\frac{dr}{d\phi} \hat{\phi} - r \hat{\mathbf{r}} \right), \quad (13)$$

where ϕ is the azimuthal angle, r is the radial distance, and $\dot{r} = dr/d\phi$. From Eq. (19) of Ref. 7 for the derivative of a brachistochrone (where ξ_d is the tangent radius of the tunnel and $\theta_d = \theta[\xi_d]$)

$$\frac{d\xi}{d\phi} = \frac{\xi}{\xi_d} \sqrt{\frac{\xi^2 \theta_d - \xi_d^2 \theta(\xi)}{\theta(\xi)}}, \quad (14)$$

the first term of the body acceleration is

$$\begin{aligned} \vec{g} \cdot \hat{\mathbf{N}} &= g(r) \hat{\mathbf{r}} \cdot \hat{\mathbf{N}} = \frac{rg}{|\dot{\mathbf{r}}|} = \frac{g}{\sqrt{\left(\frac{\xi}{\xi_d}\right)^2 \frac{\theta_d}{\theta(\xi)}}} \\ &= -4\pi G \rho_c \varepsilon \frac{d\theta}{d\xi} \frac{\xi_d}{\xi} \sqrt{\frac{\theta(\xi)}{\theta_d}}. \end{aligned} \quad (15)$$

This has the correct limits; $\vec{g} \cdot \hat{\mathbf{N}} \rightarrow 0$ near the surface (as $\xi \rightarrow \xi_0$, the normal vector is perpendicular to the radial direction and gravity acts along the curve) and $\vec{g} \cdot \hat{\mathbf{N}} \rightarrow g$ near the tangent radius (as $\xi \rightarrow \xi_d$, the normal vector is parallel to the radial direction.)

The centrifugal acceleration needs the velocity and curvature of the trajectory. Energy conservation shows that the specific kinetic energy of the projectile along the brachistochrone is proportional to θ

$$\frac{1}{2} v^2(r) = - \int_r^r g dr \Rightarrow v^2(\xi) = 8\pi G \rho_c \varepsilon^2 \theta(\xi) \quad (16)$$

(Eq. (12) of Ref. 7). This relation can be applied here, because we are ignoring any frictional drag forces, but not in the quasi-Keplerian orbits below.

Combining the identity

$$\frac{d^2 \xi}{d\phi^2} = \frac{1}{\xi} \left(\frac{d\xi}{d\phi} \right)^2 + \frac{1}{2} \left(\frac{\xi_d}{\xi} \right)^2 \left[2\xi \frac{\theta_d}{\theta} - \xi \frac{\theta_d d\theta}{\theta^2 d\xi} \right], \quad (17)$$

with the definition of the curvature in polar coordinates gives

$$\kappa = \frac{1 + 2 \left(\frac{1}{\xi} \frac{d\xi}{d\phi} \right)^2 - \frac{1}{\xi} \frac{d^2 \xi}{d\phi^2}}{\varepsilon \left[1 + \left(\frac{1}{\xi} \frac{d\xi}{d\phi} \right)^2 \right]^{3/2}} = \frac{1}{2\varepsilon\theta} \frac{d\theta}{d\xi} \frac{\xi_d}{\xi} \sqrt{\frac{\theta}{\theta_d}}. \quad (18)$$

This makes the other term of the body acceleration

$$\begin{aligned} v^2 \kappa &= 8\pi G \rho_c \varepsilon^2 \theta(\xi) \times \frac{1}{2\varepsilon\theta} \frac{d\theta}{d\xi} \frac{\xi_d}{\xi} \sqrt{\frac{\theta}{\theta_d}} \\ &= 4\pi G \rho_c \varepsilon \frac{d\theta}{d\xi} \frac{\xi_d}{\xi} \sqrt{\frac{\theta}{\theta_d}}. \end{aligned} \quad (19)$$

From here, we can use Eq. (12) to find the normal acceleration that acts outward to keep the projectile in the tunnel is

$$a_N = 2 \times 4\pi G \rho_c \varepsilon \frac{d\theta}{d\xi} \frac{\xi_d}{\xi} \sqrt{\frac{\theta}{\theta_d}} = 2 \mathbf{g} \cdot \hat{\mathbf{N}}. \quad (20)$$

The variation of the normal accelerations along the brachistochrones shown in Fig. 5 of Ref. 7 were calculated and are shown in Fig. 2 for $n=3$ polytropes scaled to reflect the Earth and Sun. The values of a_N along each trajectory are shown as black lines that converge to zero at the surface (at the right side of the figure) and rise to twice the local gravity at the tangent radius (shown by vertical dotted lines). The dashed curve is twice the value of the local gravity (g) to better show the variation of a_N . The body accelerations along brachistochrones through the Earth with tangent radii below $0.6 R_\oplus$ will exceed the hazardous limit of 6 g's (panel (a)), meaning pressure suits or other precautions would be necessary to prevent passengers from losing consciousness where the acceleration exceeds 6 g's. Accelerations in tunnels within the Sun exceed the Stapp limit for tangent radii close to the surface and have prohibitively high body accelerations along some part of the trip. However, there are paths through the solar model that do not exceed the Stapp limit, but they essentially go all the way to the core of the model. The limiting example is the curve label “Safe?” in panel (b) of Fig. 2.

V. GRAVITATIONAL POTENTIAL FOR ORBITS AROUND AND THROUGH POLYTROPES

If the body forces along brachistochrone tunnels are too great for transport, perhaps tunnels built to follow an orbital trajectory inside the object would be more suitable. Such tunnels would provide a weightless trajectory, aside from the accelerations needed at ingress and egress points, and would remain closer to the surface for easier construction. We now describe how to calculate such a trajectory. We first define the needed gravitational potential.

The enclosed mass is constant along an orbit outside a massive, spherical object, and the orbits are Keplerian to a high precision. Inside the object, however, the enclosed mass depends on the radial distance from the center. As the periaxis distance decreases the enclosed mass gets smaller, the period of the osculating orbit also decreases, and the orbit outside the object will precess in the retrograde direction. This means that the line connecting the apoapsis and periaxis appears to precess (rotate in space) opposite to the

direction of orbital motion. The force inside the polytrope remains a central force, so angular momentum continues to be a constant of motion.

The gravitational potential in Eq. (11) goes to zero at the surface of the object, which is inappropriate for orbits that can move outside the object. The surface value of the external potential must be added to the internal potential (Φ_{in}) to make Φ_{in} continuous with the r^{-1} potential outside the object, or

$$\Phi_{in} = -4\pi G \rho_c \varepsilon^2 \theta - \frac{GM_*}{\varepsilon \xi_0} = -4\pi G \rho_c \varepsilon^2 (\theta - \xi_0 \theta'_0), \quad (21)$$

while the gravitational potential outside the polytrope depends only on r^{-1}

$$\Phi_{out} = -\frac{GM_*}{\varepsilon \xi} = -\frac{4\pi G \bar{\rho} R_*^3}{3 \varepsilon \xi} = \frac{4\pi G \rho_c \varepsilon^2}{\xi} \xi_0^2 \theta'_0. \quad (22)$$

Orbits in Φ_{out} are Keplerian and can be written as conic sections. Our interest is in how the orbits outside the object merge onto the interior orbits moving through Φ_{in} . We do this by “patching” the exterior, Keplerian orbit onto the interior, quasi-Keplerian orbit at the surface. Patched orbits have a continuous magnitude and direction of the velocity vector across the surface. Thus, the exterior orbits provide the initial conditions of the interior orbits whether the projectile starts far from the object (as is the case for a star) or is accelerated at the surface (to model a transportation system). Calculating the interior orbits within polytropes have the advantage of including the $n=0$ homogeneous sphere, for which many analytic results are available, and allow the orbital properties to be determined along a smoothly varying family of mass density distributions. This made them useful as models for the motions of stars within globular clusters,²³ although potentials with simple polynomials of the radius are also used.²⁴

VI. EXTERIOR KEPLERIAN ORBITS

Although any Keplerian orbit can be used as the exterior solution to the trajectory, parabolic Keplerian orbits were

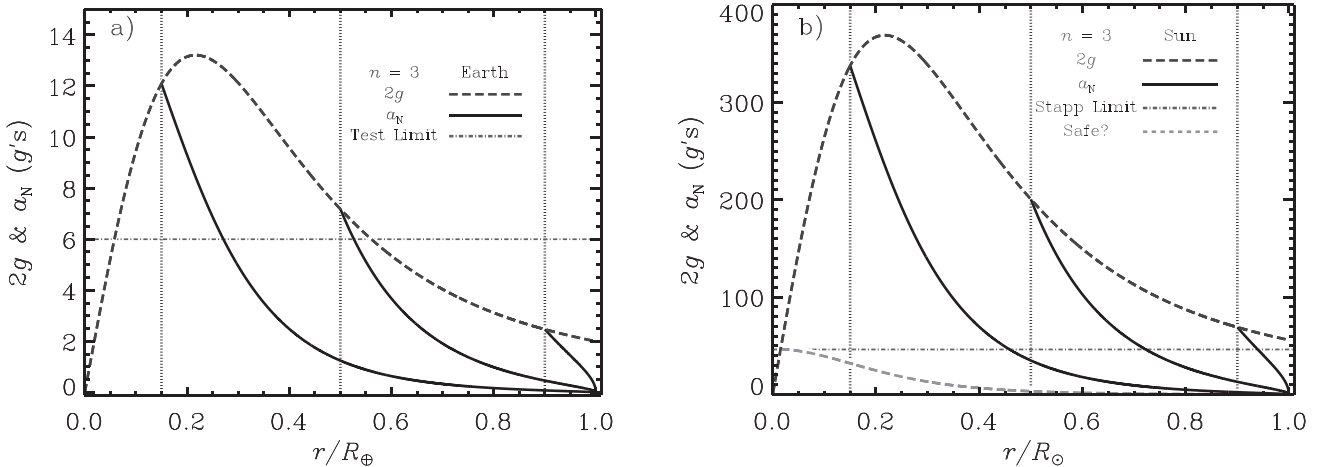


Fig. 2. The dashed curves show the variation of $2g$ in $n=3$ polytrope models scaled to represent the Earth (a, left) and Sun (b, right). The black curves show the magnitude of the normal body acceleration $a_N = 2g \cdot \dot{N}$ along brachistochrones with fractional tangent radii of 0.15, 0.5, and 0.9 (Ref. 7). The dotted-dashed line in the left plot is the Test Limit of 6 g's while the dot-dashed line in the right plot is the Stapp Survival Limit of 46.2 g's. The light dashed curve in the right plot shows a path that does not exceed the SSL, but requires reaching a fractional radius of 0.016. The vertical dotted lines indicate the tangent radii of the brachistochrones.

chosen to provide the initial conditions, such as the velocity and angle of incidence, for the interior solutions at the surface ingress point. Such orbits are completely described by a single parameter, the periapsis distance ($r_p = \epsilon \xi_p$). Elliptical orbits would provide a more general set of initial conditions, but would also add many other parameters to the discussion without greatly enhancing the physics of the problem. Any orbit passing close to the surface of the Sun can be treated as a parabola during perihelion passage. For example, sungrazing comets are often discovered too close to the Sun for a full elliptical orbit to be determined.

Parabolic Keplerian orbits moving through a hollow sphere of radius ξ_0 surrounding a point mass can also be used to validate the orbits moving through polytropes. Properties of parabolic Keplerian orbits are listed in Ref. 25, App. D.3. The important parameter is the periapsis distance normalized by the radius of the sphere, which we define to be $x_p = \xi_p/\xi_0$. The specific angular momentum, $L^2 = r_p^2 v_p^2$, where v_p is the velocity at periapsis, is a constant of the motion. For polytropes, $L^2 = 2GM_*R_*x_p = 8\pi G\rho_c \epsilon^4 \xi_p (-\xi_0^2 \theta'_0)$.

The velocity and angle of incidence of a Keplerian parabola at the surface are the initial conditions for the interior orbits. The velocity at the surface is

$$v = \sqrt{\frac{2GM_*}{R_*}} = \begin{cases} 617 & \text{km/s for the Sun} \\ 11.2 & \text{km/s for the Earth.} \end{cases} \quad (23)$$

The angle of incidence is

$$i_{para} = \arcsin(\sqrt{x_p}) \quad (24)$$

measured from the outward radial normal.

The fundamental design objective for an orbital tunnel is the angular distance traversed by the tunnel at the surface. For a parabola around a point mass, the angular distance spanned at the enclosing spherical surface is

$$\Delta\phi_{para} = 4\arccos(\sqrt{x_p}), \quad (25)$$

and is shown in Fig. 3 for $0 < x_p < 1$. Because points with $\Delta\phi > \pi$ can be considered separated by $2\pi - \Delta\phi$, this

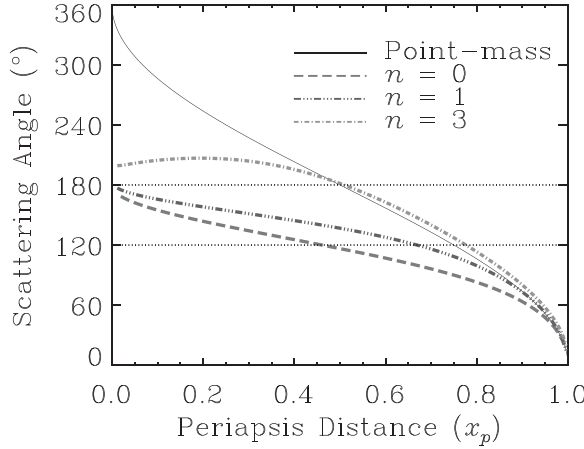


Fig. 3. The variation of the angular distance at the surface with normalized parabolic periapsis distance for the interior solutions (various linestyles) and the Keplerian parabola (solid line). The polytropic indices are identified by line type in the legend. Two horizontal dotted lines show angles of 120° and 180°. The former is drawn to show solutions suitable for Fig. 1; the latter is the symmetry line above which the angular distance can be recast as $360^\circ - \Delta\phi$.

distance is double valued, but will be displayed in its full range below. As the periapsis distance approaches the surface the incoming orbit only skims the surface while small periapses imply a near-vertical entry.

The next important quantity is how long it takes to traverse the tunnel. The time of flight along a parabolic orbit, measured from ingress to egress, is twice the time from periapsis to the surface

$$\Delta T_{para} = 2T_0 (1 - x_p)^{1/2}(1 + 2x_p)/3 \text{ (sec)}, \quad (26)$$

where $T_0 = \sqrt{2R_*^3/GM_*} = 2253$ s for the Sun and 1140 s for the Earth. The travel times for parabolic Keplerian orbits around a point mass with the mass of the Earth are shown as a solid line in Fig. 4. The traversal times as a function of angular distance along a parabolic Keplerian orbital tunnel are double valued for all periapsis distances, $0 < x_p < 1$. The angles shown in Fig. 3 vary from 0 to 360°, but for $\Delta\phi > 180^\circ$ the angular distance should be recast as $360^\circ - \Delta\phi$. There is a short time path between surface points connected by a trajectory with $x_p > 0.865$ and a long path. The former becomes very short as $x_p \rightarrow 1$ but the other has to move to the center and back, so the times become roughly constant as $x_p \rightarrow 0$. This 13 min traversal time is less than half of the fall-through time in Table I because they enter the object moving at 11.2 km/s rather than from rest.

VII. INTERIOR QUASI-KEPLERIAN ORBITS

We now describe how an incoming parabolic Keplerian orbit is modified as the projectile moves through polytropes with $n = 0, 1$, and 3. Only the interior solutions need to be generated as external Keplerian parabolas are patched onto the interior orbits at the ingress and egress points on the surface. The calculated angular distance will be compared with that of a Keplerian parabola in Eq. (25) and the traversal times with the time-of-flight in Eq. (26). We will call the minimum of the quasi-Keplerian orbit the achieved periapsis (ξ_1) to distinguish it from the periapsis (ξ_p) of the exterior parabolic orbit. Analytic solutions for the $n = 0$ orbits and

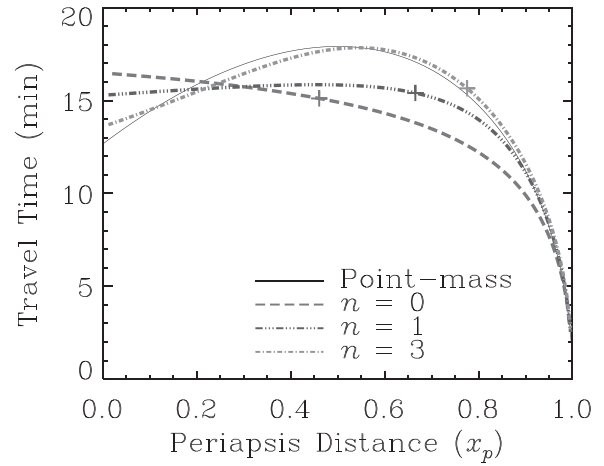


Fig. 4. The variation of the traversal time with radial distance for the interior solutions and the Keplerian time-of-flight (solid line labeled Point-mass) through models scaled to the Earth. The polytropic indices are identified by line type in the legend. Plus signs ('+') are drawn at the transit times of the 120° trajectories for the interior solutions used in Fig. 1.

Table II. Achieved periapsis and apoapsis distances for $n = 0$.

Regime	ξ_1/ξ_0	ξ_{\max}/ξ_0
$x_p \ll 1$	$2\sqrt{x_p/6}$	$\sqrt{3}$
$x_p \approx 1$	$\sqrt{x_p}$	$\sqrt{2x_p}$

traversal times will be presented and used to test the numerical realizations.

The equations of motion for a particle moving in the potential of Eq. (21) reduce to

$$\frac{d\phi}{d\xi} = \frac{1}{\xi} \left[\frac{2(E - \Phi_{\text{in}})\xi^2}{L^2} - 1 \right]^{-1/2}. \quad (27)$$

As parabolic orbits have $E = 0$, the equation of motion for the interior solution becomes

$$\frac{d\phi}{d\xi} = \frac{1}{\xi} \left[\frac{-\xi_p \xi_0 \theta'_0}{(\theta - \xi_0 \theta'_0) \xi^2 + \xi_p \xi_0^2 \theta'_0} \right]^{1/2}. \quad (28)$$

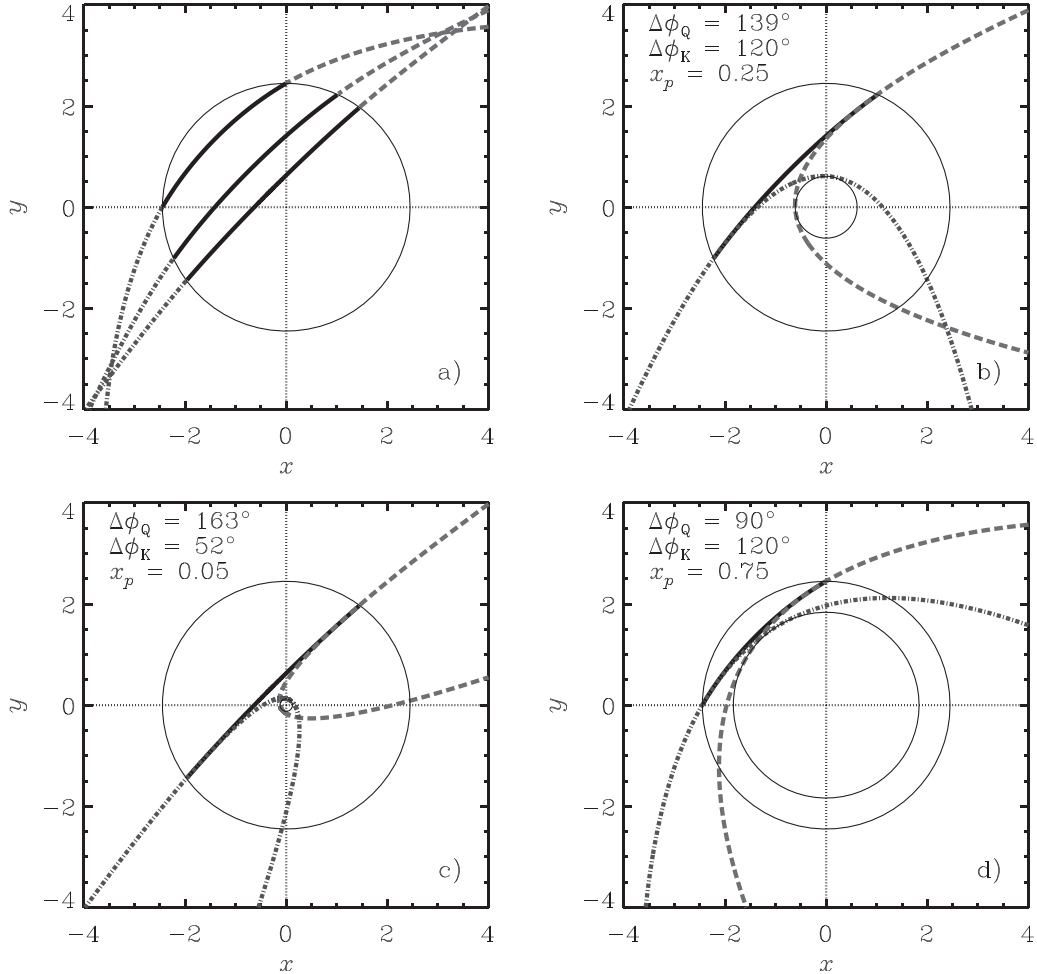


Fig. 5. Three quasi-Keplerian orbits passing through an $n = 0$ polytrope with the projectile moving inward from the upper right. The incoming parabolic periapsis distances are $x_p = 0.05, 0.25$, and 0.75 . The upper left panel (a) shows the patched conic section orbits. The upper right panel (b) shows the two parabolas that are fitted to the entry and exit points of the $x_p = 0.25$ example. The lower left (c) is the $x_p = 0.05$ and the lower right (d) is the $x_p = 0.75$. Solid lines show the interior quasi-Keplerian orbit while dashed lines show the incoming path and dot-dashed lines the outgoing path. The legends show the angular distance traversed at the surface by the quasi-Keplerian ($\Delta\phi_Q$) and parabolic ($\Delta\phi_K$) orbits, along with the value of x_p . Thin circles are drawn at the surface radius of the object in all panels and at x_p in the appropriate panels.

Numerical integration of this equation is necessary for $n > 0$. Near the achieved periapsis, where the denominator in Eq. (28) is zero, it is necessary to expand the denominator and get an analytic solution to initialize the numeric solution.

The traversal time is twice the time it takes to travel from the achieved periapsis to the surface

$$\begin{aligned} \Delta\tau &= 2 \int_{r_1}^{R_*} \frac{dr}{v} \left[1 + \left(r \frac{d\phi}{dr} \right)^2 \right]^{1/2} \\ &= 2T_p \int_{\xi_1}^{\xi_0} \frac{d\xi}{\xi_0} \left[\frac{\xi^2}{\xi^2(\theta - \xi_0 \theta'_0) + \xi_p \xi_0^2 \theta'_0} \right]^{1/2}, \end{aligned} \quad (29)$$

where $v^2 = 8\pi G \rho_c \epsilon^2 (\theta - \xi_0 \theta'_0)$ and $T_p = \xi_0 / \sqrt{8\pi G \rho_c} = T_0 \sqrt{-\xi_0 \theta'_0} / 2$.

Solutions of Eq. (29) must also be numerically integrated for $n > 0$. Near ξ_1 (where the denominator is zero) the numerical integration needs a starter value. This is given by integrating a linear expansion of Eq. (29) near ξ_1 .

A. Interior orbits through an $n = 0$ polytrope

An analytic solution is available for the interior orbits of the $n = 0$ polytrope, and we will sketch that to introduce the concepts for the general case. Substituting $-\xi_0 \theta'_{\xi_0} = 2$ and introducing the $n = 0$ solution into the potential in Eq. (28) gives

$$\frac{d\phi}{d\xi} = \frac{1}{\xi} \left[\frac{2\xi_p \xi_0}{3\xi^2 - \xi^4/\xi_0^2 - 2\xi_p \xi_0} \right]^{1/2}. \quad (30)$$

Defining $u = (\xi/\xi_0)^2$ and $du/u = 2d\xi/\xi$, we have

$$\frac{d\phi}{du} = \frac{1}{2u} \sqrt{2x_p} \left[\frac{1}{3u - u^2 - 2x_p} \right]^{1/2}. \quad (31)$$

Using integral 2.266 of Ref. 26 gives

$$\sin(2\phi) = \frac{3 - 4x_p/u}{\sqrt{9 - 8x_p}} \quad (32)$$

and then transforming back to ξ gives the interior orbit

$$\xi^2 = \frac{4x_p \xi_0^2}{3 - \sqrt{9 - 8x_p} \sin(2\phi)}. \quad (33)$$

This is the equation for an ellipse, centered on the origin and with the semi-major axis rotated -45° as described in Ref. 27. Simoson²⁸ provides an orbit with the semi-major axis aligned along the y axis. Those orbits are tangent to the interior surface of the Earth and cannot be used for the orbital tunnels described here. If the initial conditions are expanded to include an incoming ellipse, the orbits described here coincide with those of Ref. 28 for an initial horizontal velocity value of the Earth's surface rotation velocity.²⁹

The achieved periapsis distance is now given by the minimum values of Eq. (33), when $\phi = -45^\circ$ and 135°

$$\xi_1 = \xi_0 \sqrt{\frac{4x_p}{3 + \sqrt{9 - 8x_p}}}. \quad (34)$$

Expanding the definition of the orbital radius [Eq. (33)] in the limits of very small parabolic periapsis distances $x_p \ll 1$

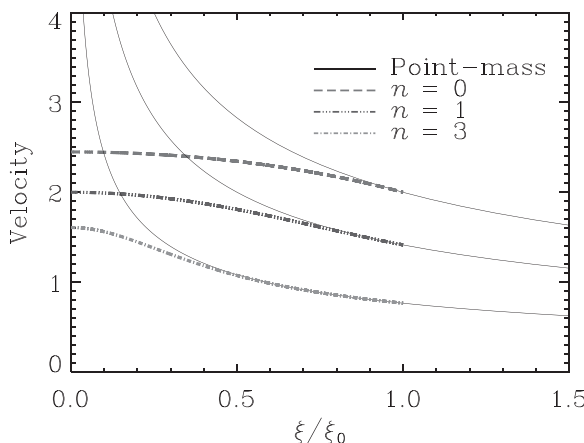


Fig. 6. The variation of the velocity with radial distance for the interior solutions (solid colored lines) and the Keplerian velocity (dashed lines). The velocities are normalized by $\sqrt{4\pi G\rho_c e^2}$, which shifts them vertically to show the separate curves. The polytropic indices are identified by line type in the legend.

and for $x_p \approx 1$, we can produce a table of the dependence of the maximum and minimum orbital radii on x_p (Table II).

As a result of the boundary condition that the interior orbit matches an exterior parabola, these interior orbits are not completely inside the polytrope, the apoapsis can reach a radius of $\sqrt{3} \xi_0$! However, only the interior solution is used in the patched orbits presented below.

Three examples of tunnels through $n = 0$ polytropes that match parabolas outside the object are shown in Fig. 5. A Keplerian parabolic orbit with a periapsis distance of ξ_p pierces the surface and is matched to the appropriate interior solution. When the interior solution reaches the surface on the other side of the object, another parabola is patched on. These different phases are detailed in Fig. 5. By comparing the solid initial orbits with the dashed exiting orbits, you can see that these orbits suffer an apparent retrograde motion of the orbit as they pass through the object. For example, if the projectile continued along the initial parabola in the $x_p = 0.25$ example, it would exit the plot at $(4.0, -2.9)$; but after passing through the polytrope it exits at $(-4, -4)$. The scattering angle changed from -36° to -135° , an retrograde change of 99° .

As shown in Fig. 5, the softening of the gravitational acceleration as the object passes closer to the center causes a greatly reduced scattering angle. This results in tunnels that can only access the opposite side of the object. The closer to the center the tunnel passes, the closer to a straight line the trajectory becomes. As shown in Fig. 6, the velocity is much lower along these orbits as well.

The angular distance traversed along the surface is the distance between the points where the interior solution crosses the surface is

$$\Delta\phi_{n=0} = \pi - 2\phi_s = \arccos\left(\frac{4x_p - 3}{\sqrt{9 - 8x_p}}\right), \quad (35)$$

because $\sin(2\phi_s) = (3 - 4x_p)/\sqrt{9 - 8x_p}$ (from Eq. (32)). The angular distances for the interior trajectories were calculated for $0 < x_p < 1$ and are shown as a dashed line in Fig. 3. The angular distance traveled by the $n = 0$ interior trajectory

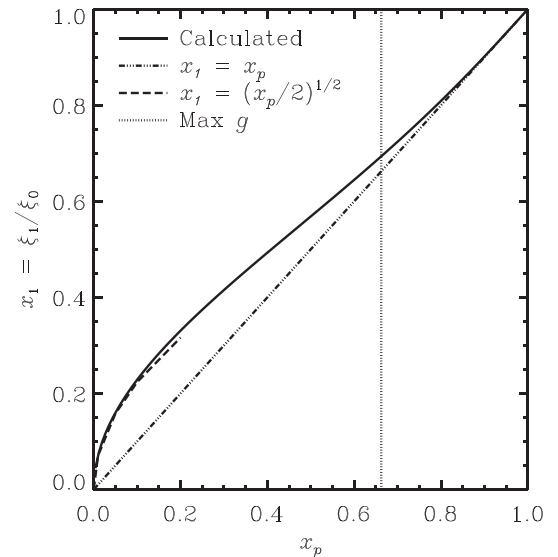


Fig. 7. The dependence of the normalized achieved periapsis ($x_1 = \xi_1/\xi_0$) with the periapsis of the incoming parabolic orbit (x_p) for an $n = 1$ polytrope. The calculated achieved periapsis is shown as a black solid line, an approximation for small periapses as a dashed line, the line of equality as a chain-dashed line, and the location of the maximum in g is plotted as a vertical dotted line.

is dramatically different from that of the parabolic Keplerian orbit. The interior orbits do not deflect the projectile as x_p decreases; rather, the projectile flies through the polytrope without deflection as $x_p \rightarrow 0$.

The travel time of quasi-Keplerian interior orbits in a $n=0$ polytrope can also be written as a function of x_p . Putting the $n=0$ potential into Eq. (29), we have

$$\Delta\tau(x_p) = 2T_p \int_{\xi_1}^{\xi_0} \frac{d\xi}{\xi} \xi \left[\frac{1}{3\xi^2 - \xi^4/\xi_0^2 - 2x_p \xi_0^2} \right]^{1/2}, \quad (36)$$

where with ξ_1 the positive zero of the denominator. Substituting $u = \xi^2$, setting $a = -2x_p \xi_0^2 = -12x_p$, $b = 3$, $c = -1/\xi_0^2$, $\Delta = 4ac - b^2 = 8x_p - 9 < 0$, and using integral 2.261,²⁶ we get the travel time

$$\begin{aligned} \Delta\tau &= \frac{T_p}{\xi_0} \int_{u_1}^{u_0} \frac{du}{\sqrt{a + bu + cu^2}} \\ &= -\frac{T_p}{\xi_0 \sqrt{-c}} \arcsin \left(\frac{2uc + b}{\sqrt{-\Delta}} \right) \Big|_{u_1}^{u_0} \\ &= T_p \arccos \left(1/\sqrt{9 - 8x_p} \right). \end{aligned} \quad (37)$$

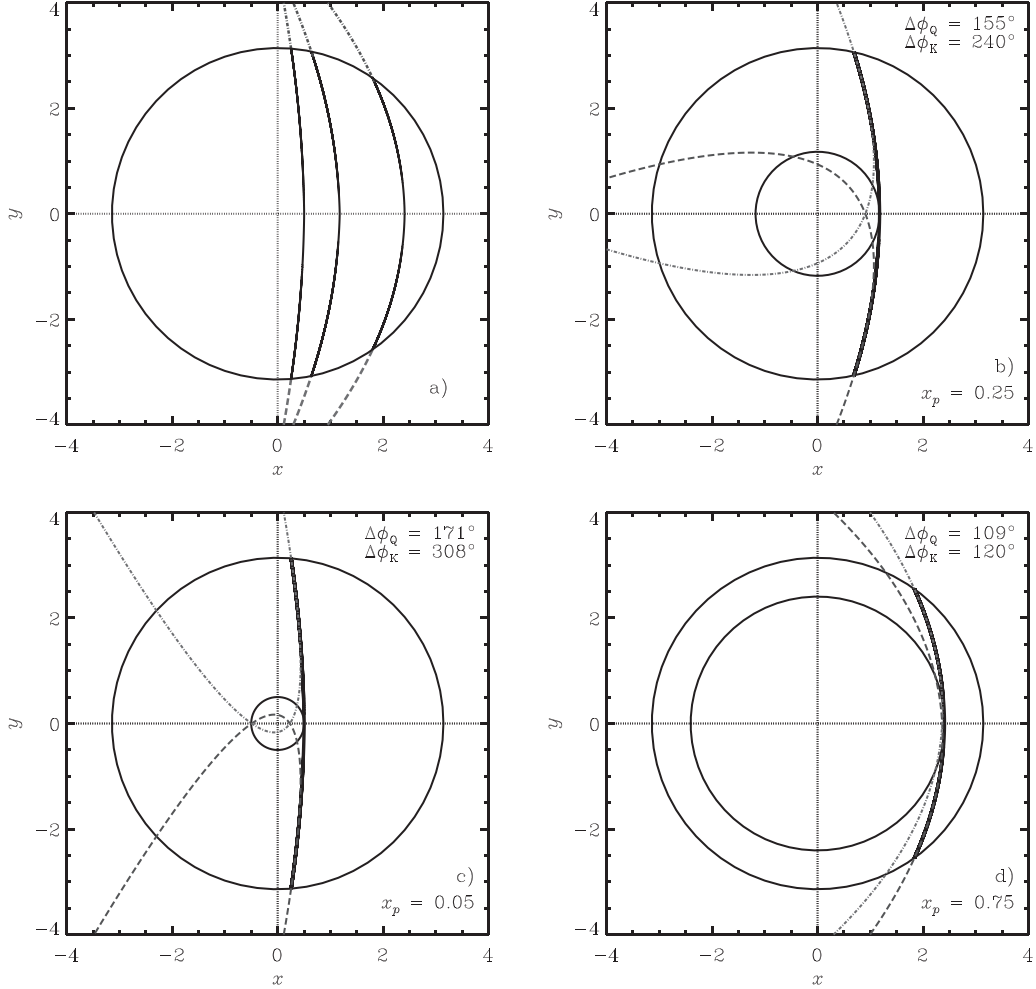


Fig. 8. Three quasi-Keplerian orbits passing through an $n=1$ polytrope, moving upwards through the object. The incoming parabolic periaxis distances are $x_p = 0.05, 0.25$, and 0.75 . In all panels, the interior orbit is a solid line. The upper left panel (a) shows the patched conic section orbits. The upper right panel (b) shows the two parabolas that are fitted to the entry and exit points of the $x_p = 0.25$ example. The lower left (c) is the $x_p = 0.05$ and the lower right (d) is the $x_p = 0.75$. Dashed lines show the incoming parabolas and dot-dashed lines the outgoing. The legends show the angular distance traversed at the surface by the quasi-Keplerian ($\Delta\phi_Q$) and parabolic ($\Delta\phi_K$) orbits, along with the value of x_p in the lower right corner. Thin circles are drawn at the surface radius of the object in all panels and at x_p in the appropriate panels.

Putting in the scaling factors for the Earth gives

$$\Delta\tau = 806.1 \arccos(1/\sqrt{9 - 8x_p}) \text{ s}, \quad (38)$$

which is shown as a dashed line in Fig. 4. These curves agree well enough with the numeric results that only one is shown. The interior quasi-Keplerian orbit takes less time than a brachistochrone but a similar time to the Keplerian parabola. Both of these can be understood by the variation in the velocity. The Keplerian parabola continues to accelerate as it moves toward the point mass at the center. The velocity of the modified interior orbit reaches a maximum velocity. Thus, the modified orbit moves about the same distance at a slower speed and hence moves the same angular distance more slowly than a Keplerian parabola for small x_p . The brachistochrone is slower because it starts at rest and builds up speed as it moves down into the object.

B. Interior orbits through a generic polytrope

We now describe the numerical solutions of the interior orbits for the $n=1$ and $n=3$ polytropes. The integrations start at the achieved periapsis and end at the surface, where a

parabola is patched to continue the trajectory outside the object. Throughout the $n = 1$ model the achieved periapsis (ξ_1), which is the position of the zero of the denominators in Eqs. (28) and (29), is greater than the periapsis of the incoming parabola. This is illustrated in Fig. 7, where the calculated periapsis and two approximations are shown. A similar plot can be made for the $n = 3$ polytrope.

We can now build orbital tunnels through $n = 1$ polytropes that match parabolas outside the object. Three examples using the same values of x_p as in Fig. 5 are shown in Fig. 8. Each orbit follows the same scenario. A parabolic Keplerian orbit with a periapsis distance of ξ_p pierces the surface and is matched to the appropriate interior solution. When the interior solution reaches the surface on the other side of the object, another parabola is patched on. These different phases are detailed in Fig. 8. These orbits also suffer an apparent retrograde motion (precession) of the orbit as they pass through the object.

The trajectories from both the $n = 0$ and $n = 1$ polytropes show how the object acts as a lens and focuses the orbits, which would otherwise disperse over a wide angle. Orbits around a point mass show a large angular deflection as $x_p \rightarrow 0$. By contrast, the $n = 0$ and $n = 1$ trajectories show no deflections greater than 180° , as can be seen in Fig. 3.

Orbital tunnels through $n = 3$ polytropes that match parabolas outside the object using the same values of x_p as in Fig. 5 are shown in Fig. 9. As with the $n = 0$ and $n = 1$ polytropes, these orbits suffer an apparent retrograde motion of the orbit as they pass through the object. However, the angular distance tends to track the Keplerian parabola until periapsis is deeper in the object (Fig. 3) and the time to traverse the object tracks that of the Keplerian parabola, but with a longer traversal time near the core (Fig. 4).

Compared to the Keplerian parabolas, orbits through polytropes tend to (1) have similar traversal times for the same incoming periapsis distance, (2) span a smaller angular distance for $n = 0$ and 1 with a similar incoming parabolic periapsis distance, but (3) span a similar angular distance for $n = 3$ for $x_p > 0.5$ while diverging in angular distance for $x_p < 0.5$. Although orbital tunnels through the Earth take less time than a brachistochrone trajectory, they require accelerating the payload to orbital velocities before entering the tunnel. It is also necessary to stop the payload at the far end of the trajectory. You trade the large body forces of the brachistochrone for enormous accelerations at both ends of the trip.

As an example, let us examine the burrito delivery tunnel mentioned in the Introduction. The angular distance from San Francisco, CA, to New York City, NY, is 38° ,

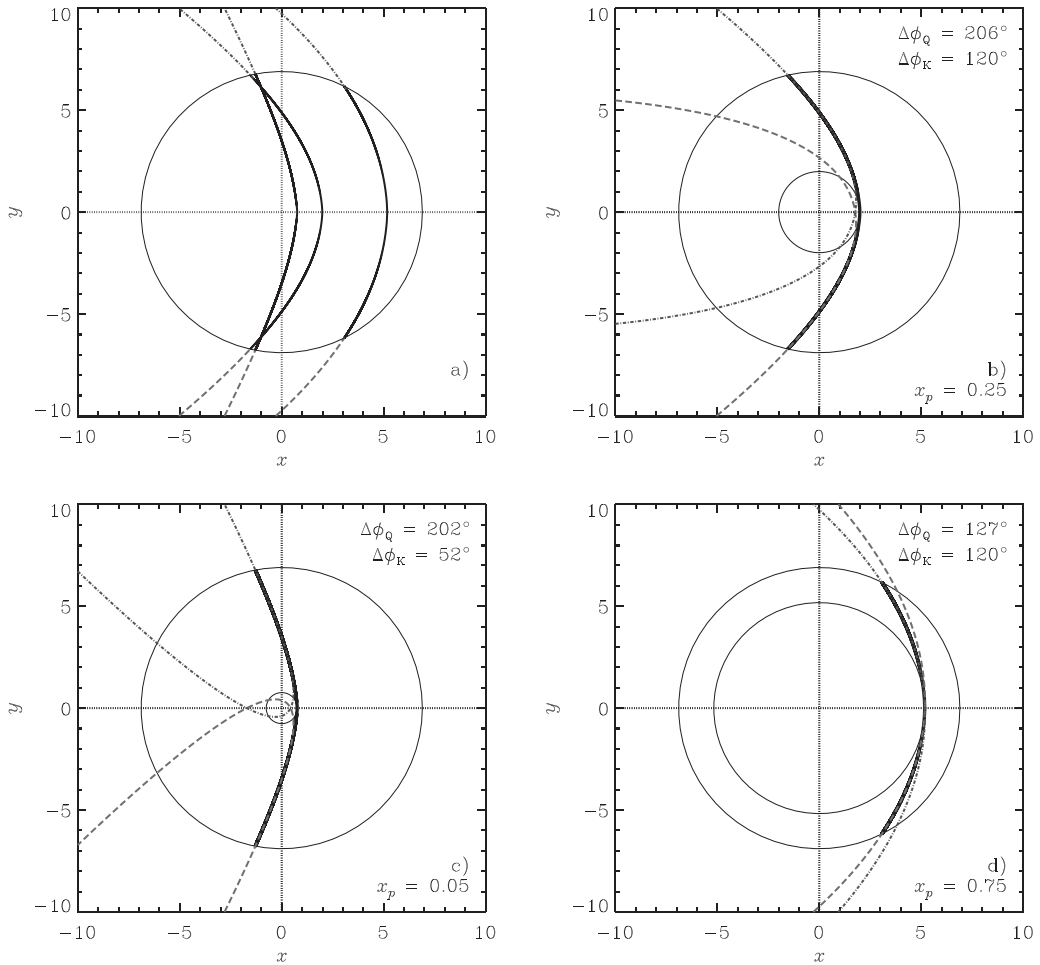


Fig. 9. Three quasi-Keplerian orbits passing through an $n = 3$ polytrope, moving upwards through the object. The incoming parabolic periapsis distances are $x_p = 0.05, 0.25$, and 0.75 . The upper left panel (a) shows the patched conic section orbits. The upper right panel (b) shows the two parabolas that are fitted to the entry and exit points of the $x_p = 0.25$ example. The lower left (c) is the $x_p = 0.05$ and the lower right (d) is the $x_p = 0.75$. Dashed lines show the incoming path and dot-dashed lines the outgoing path. The legends show the angular distance traversed at the surface by the quasi-Keplerian ($\Delta\phi_Q$) and parabolic ($\Delta\phi_K$) orbits, along with the value of x_p . Thin circles are drawn at the surface radius of the object in all panels and at x_p in the appropriate panels.

Table III. Angular distances traversed by quasi-Keplerian orbits tuned to the earth.

x_p	Parabola		$n = 0$		$n = 1$		$n = 3$	
	$\Delta\phi_K$ (deg)	τ (min)	$\Delta\phi_Q$ (deg)	τ (min)	$\Delta\phi_Q$ (°)	τ (min)	$\Delta\phi_Q$ (deg)	τ (min)
0.05	308	13.6	163	16.4	171	15.4	165	14.0
0.25	120	16.5	139	15.9	155	15.7	160	16.0
0.75	120	15.8	90	12.9	109	14.7	122	16.2

corresponding to a distance of 4225 km along a sphere with a radius of the mean radius of the Earth ($R_\oplus = 6371$ km). An $n=0$ orbital tunnel spanning this angle would be initialized with the surface values of an incoming Keplerian parabola with $x_p = 0.9696$, reach an achieved periapsis of $0.9710 R_\oplus$ (a maximum depth of 185 km) at the halfway point, and would be traversed in 6.2 min. While that sounds attractive, the time to accelerate the burrito to an initial velocity of 11 km/s with a constant acceleration of 6 g's is 3.1 min, with a similar time needed to slow the burrito at the other end. And it would require 1010 km of acceleration at each end of the tunnel. The payload would be under high acceleration for almost 50% of the journey. You can increase the acceleration but the limits of 6 g's used for spacecraft manufacturing may be the practical maximum for safely transporting organic material such as humans and burritos (Table III).

Therefore, these tunnels may not be an effective transport system on the Earth. That does not mean they shouldn't be considered for tunnels through stars and groups of stars, which are intended only for gathering data about the interior of the star or group. This is discussed in Sec. VIII.

VIII. TRAVERSAL TIMES OF BRACHISTOCHRONE AND ORBITAL TUNNELS THROUGH THE SUN

As described in Sec. IV, brachistochrone tunnels are an impossible path for a satellite moving through a star, because the normal forces exerted by the walls of the tunnel would most likely shatter the instruments on the satellite. Such a path is made even more difficult because walls can't exist in the gaseous interior of a star, or even the quasi-molten interior of a terrestrial planet. By contrast, particles traveling without drag along quasi-Keplerian orbits through the Sun would experience lower body forces and could provide less mechanically strenuous orbital options.

Table IV provides the traversal times for three brachistochrone tunnels and three orbital tunnels that enter and exit

Table IV. Properties of trajectories through the sun for selected angular distance.

$\Delta\phi^a$ (deg)	Brachistochrone ^a		Keplerian Parabola ^b		$n = 0$ Interior ^c		$n = 3$ Interior ^d	
	x_p	ΔT (min)	x_p	ΔT (min)	x_p	ΔT (min)	x_p	ΔT (min)
16.9	0.90	34.2	0.9946	5.52	0.9944	5.51	0.9975	4.53
70.7	0.50	53.6	0.9093	21.3	0.8684	21.2	0.9222	20.6
131.	0.15	55.4	0.7074	32.8	0.3386	30.8	0.7350	32.4

^a $n = 3$ values from Table II of Ref. 7, $\Delta T = \tau \times \sqrt{\bar{\rho}_\oplus / \bar{\rho}_\odot}$.

^bFrom Eqs. (25) and (26).

^cFrom Eqs. (35) and (38), achieved periapsis is 0.5.

^dNumerical integration of Eqs. (28) and (29).

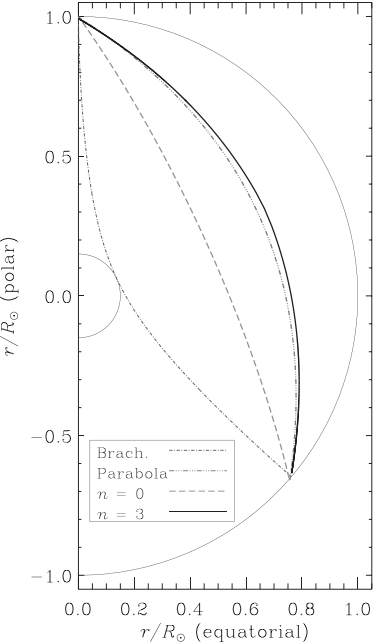


Fig. 10. The brachistochrone and orbital tunnels listed in Table IV for an angular distance of 131° . The shade and style of the lines is mapped to the different orbital tunnels in the legend. All radial positions were normalized by the outer radius (the large, thin, solid black line). The tangent radius of the brachistochrone is shown by a thin black semicircle at $r_d/R_\odot = 0.15$.

the Sun at the same points. The brachistochrone traversal times are taken from the last row of Table II (Ref. 7) and were scaled by 1.97 to account for the difference in the average densities of the Earth and Sun. The Keplerian parabola traversal times are from Eq. (26), scaled to solar values. In general, a satellite would spend less time inside the Sun if traveling along an orbital tunnel than along a brachistochrone connecting the same points at the surface. The shortness of the $\Delta\phi = 17^\circ$ traversal time is due to the enormous velocity of the parabola in an orbit that skims the outer layers of the Sun. The distance along the arc is 2.1×10^5 km, which would be traversed in 5.8 min by a projectile moving at 600 km/s, which supports with the calculated traversal time.

Figure 10 shows how quasi-Keplerian orbits provide alternatives to brachistochrone tunnels for traversing an angular distance of 131° . They show the advantage of orbital tunnels—the trajectories are much closer to the surface than a brachistochrone spanning the same angular distance at the surface. Because of the higher initial and average velocity it also takes less time to traverse the orbital tunnel. These orbits would be gravitationally accelerated by the Sun as they approach, rather than requiring the enormous accelerations from rest of the Earth transport system described in Sec. VII. So the paths can be realized if the payload can be steered into the correct incoming parabolic Keplerian orbit.

IX. CONCLUSIONS

We have shown that polytropes provide a way to calculate orbital tunnels within the Earth, the Sun, and other celestial bodies along a family of mass density distributions with varying central condensations. We used those polytropes to calculate orbits that allow a craft to move from one point on the surface to another with initial conditions at the surface entry point derived from Keplerian parabolas. We have

linked models of planets to models of stars by looking at how the variation of the interior gravity changes the motions of particles moving through the models.

We have also shown that objects moving along brachistochrone tunnels through a planet or star will experience very large body forces. The magnitude of the normal force needed to maintain the trajectory increases quickly when the object travels through the Sun, reaching g levels above the Stapp Survival Limit of 46.2 g 's only 5% of a solar radius below the surface. Quasi-Keplerian orbits through a mass do not experience large body forces. However, for the same angular distance traveled at the surface as the brachistochrones, they require initial velocities on the order of the escape velocity. It was also shown that the changing potential energy inside the polytrope results in a retrograde precession of the orbital path as viewed by an external observer.

Compared to the Keplerian parabolas that form their initial conditions, quasi-Keplerian orbits through polytropes with the same periapsis distance tend to (1) be slower, (2) require a similar amount of time to move the same angular distance, and (3) span a similar angular distance for periapses near the surface but do not show the reversal seen in the parabolas for small periapsis distances.

If we compare quasi-Keplerian orbits to brachistochrones that span the same angular distance at the surface, the orbital tunnels tend to (1) be faster, (2) stay closer to the surface, and (3) take less time to move the same angular distance. Although orbital tunnels through the Earth take less time than a brachistochrone trajectory, they require accelerating the payload to orbital velocities before entering the tunnel. It is also necessary to stop the payload at the far end of the trajectory. You trade the large body forces of the brachistochrone for enormous accelerations at both ends of the trip. Hence, these tunnels may also not be an effective transport system on the Earth. A hybrid transport system using trains in a vacuum tunnel that follows a parabolic trajectory over the Earth may be a usable compromise.

Rotation is one complication that should be included in these imagined journeys through the Earth and Sun. Simoson³⁰ has examined how gravity trains are affected by the rotation of the Earth. One essential conclusion is that the tunnels cannot be used for two-way travel. To the extent that the traversal times are smaller for orbital tunnels than gravity trains, the rotational effects will be reduced. These effects would be smaller for the slowly rotating Sun, but our interest there is in sampling the interior of the Sun on a one-time pass.

Imagining a vacuum tunnel can be carved through the interior of the Earth or Sun may seem like an impossible, purely theoretical problem. However, the homogeneous sphere (or $n=0$ polytrope) potential is a model of quark motions, although the quarks cannot escape. Stars moving through the core of a globular cluster would follow trajectories that look similar to the orbits calculated in Secs. VII and VIII.⁸ Additionally, if the quasi-Keplerian orbits were followed through an entire orbit they would resemble the paths of WIMPs moving into and out of the Sun.⁹

The focussing effects seen in the trajectory plots for low central condensation may mean stars in a globular cluster could focus WIMPs emitted by their parent galaxy in our direction as the cluster passes between the Earth and the galaxy. This focussing effect could increase the flux of WIMPs from the galaxy and increasing the probability of their detection. The small scattering angles of projectiles moving

through polytropes with low central condensation (here $n=0$ or 1) are similar to the scattering of the Thomson Plum Pudding model of the atom. Although the Rutherford model of a near-point nucleus is appropriate to atomic physics, WIMPs could probe the softer potential in the central regions of globular clusters. Accidental alignments between WIMP-emitting galaxies, an orbiting globular cluster, and a detector on Earth may increase the observed WIMP signal. Unlike the general relativistic effects that form gravitational lenses and focus photons, non-relativistic particles would be affected by the changes in the internal gravitational potential described here.

Another example is the excitation of p -modes by the passage of a primordial black hole through the Sun.¹¹ The innermost parabolic orbit those authors assumed for the black hole trajectory ($x_p=0.5$) does not appear to account for the change in mass with distance, which is appropriate for that perihelion distance. If the perihelion distance were any smaller, then the effects considered here should be included and the production of p -modes would be reduced by the slower velocity of the primordial black hole.

Constructing orbital tunnels in the Earth may be simpler because they tend to be closer to the surface than a brachistochrone spanning the same distance. Even though the normal force can be too large in magnitude for a projectile to survive a trip along a brachistochrone curve through the Earth or Sun, the quasi-Keplerian orbits require the projectile to travel at very high speeds. Thus, the accelerations required at both ends of the quasi-Keplerian tunnel may also make them unsuitable for transportation between points on the Earth's surface.

ACKNOWLEDGMENTS

The authors gratefully acknowledge the support of NASA's Solar Dynamics Observatory. The authors thank the referees for useful suggestions and for pointing out the previous work of Simoson.

^aElectronic mail: William.D.Pesnell@NASA.gov

¹Paul W. Cooper, "Through the earth in forty minutes," *Am. J. Phys.* **34**(1), 68–70 (1966).

²Maciej Ceglowski, "The Alameda-Weehawken Burrito tunnel," (2007); <http://www.idlewords.com/2007/04/the_alameda_weehawken_burrito_tunnel.htm>.

³Giulio Venezian, "Terrestrial brachistochrone," *Am. J. Phys.* **34**(8), 701 (1966).

⁴Elon Musk, "Hyperloop alpha," Technical Report, SpaceX, 2013; <http://www.spacex.com/sites/spacex/files/hyperloop_alpha.pdf>.

⁵A. R. Klotz, "The gravity tunnel in a non-uniform earth," *Am. J. Phys.* **83**(3), 231–237 (2015).

⁶A. R. Klotz, "A guided tour of planetary interiors," e-print [arXiv:1505.05894](https://arxiv.org/abs/1505.05894) [physics.pop-ph].

⁷W. D. Pesnell, "Flying through polytropes," *Am. J. Phys.* **84**, 192–201 (2016).

⁸F. C. Adams and A. M. Bloch, "Orbits in extended mass distributions: General results and the spirographic approximation," *Astrophys. J.* **629**, 204–218 (2005).

⁹S. Sivertsson and J. Edsjö, "Accurate calculations of the WIMP halo around the Sun and prospects for its gamma-ray detection," *Phys. Rev. D* **81**(6), 063502 (2010).

¹⁰D. T. Cumberbatch, J. A. Guzik, J. Silk, L. S. Watson, and S. M. West, "Light WIMPs in the Sun: Constraints from helioseismology," *Phys. Rev. D* **82**(10), 103503 (2010).

¹¹M. Kesden and S. Hanasoge, "Transient solar oscillations driven by primordial black holes," *Phys. Rev. Lett.* **107**(11), 111101 (2011).

¹²S. Chandrasekhar, *An Introduction to the Study of Stellar Structure* (Dover, New York, 1967).

¹³W. D. Pesnell, "Properties of Eötvös spheres," *Astrophys. J.* **344**, 851–855 (1989).

- ¹⁴W. D. Pesnell, "Weight functions in adiabatic stellar pulsations. I-Radially symmetric motion," *Astron. Soc. Pacific* **99**, 975–985 (1987).
- ¹⁵Brent Y. Creer, Harald A. Smedal, and Rodney C. Wingrove, "Centrifuge study of pilot tolerance to acceleration and the effects of acceleration on pilot performance," Technical Report, NASA-TN-D-337, NASA, Washington, DC, 1960; <<http://ntrs.nasa.gov/archive/nasa/casi.ntrs.nasa.gov/19980223621.pdf>>.
- ¹⁶Highest g-force on a roller coaster, 2017. <https://coasterpedia.net/wiki/Highest_g-force_on_a_roller_coaster>.
- ¹⁷14 CFR 23.562—Emergency landing dynamic conditions, 2011. <<https://www.law.cornell.edu/cfr/text/14/23.562>>.
- ¹⁸Nick T. Spark, 46.2 Gs!! The Story of John Paul Stapp, the Fastest Man on Earth, 2004. <<http://www.ejectionsite.com/stapp.htm>>.
- ¹⁹NASA, "Payload vibroacoustic test criteria," Technical Report NASA-STD-7001A, NASA, 2011.
- ²⁰Ian R. McNab, "Launch to space with an electromagnetic railgun," *IEEE Trans. Mag.* **39**, 295–304 (2003).
- ²¹Tracy Frost, "Survivable electronics for control of hypersonic projectiles under extreme acceleration," 2011. <http://www.navysbir.com/n12_1/N121-102.htm>.
- ²²L. Jackson Laslett, "Trajectory for minimum transit time through the earth," *Am. J. Phys.* **34**(8), 702–703 (1966).
- ²³H. C. Plummer, "On the problem of distribution in globular star clusters," *Mon. Not. R. Astron. Soc.* **71**, 460–470 (1911).
- ²⁴W. Dehnen, "A family of potential-density pairs for spherical galaxies and bulges," *Mon. Not. R. Astron. Soc.* **265**, 250–256 (1993).
- ²⁵James R. Wertz, *Mission Geometry; Orbit and Constellation Design and Management*, Space Technology Library Vol. 13 (Microcosm & Springer, El Segundo, Cali., 2001).
- ²⁶I. S. Gradshteyn and I. M. Ryzhik, *Table of Integrals, Series and Products* (Academic, New York, 1965).
- ²⁷Aaron K. Grant and Jonathan L. Rosner, "Classical orbits in power-law potentials," *Am. J. Phys.* **62**(4), 310–315 (1994).
- ²⁸Andrew J. Simoson, "Falling down a Hole through the Earth," *Math. Mag.* **77**(3), 171–189 (2004).
- ²⁹W. Dean Pesnell, "The flight of Newton's cannonball," *Am. J. Phys.* **86**, 338–343 (2018).
- ³⁰Andrew J. Simoson, "Sliding along a chord through a rotating Earth," *Am. Math. Month.* **113**, 922–928 (2006).



Savart's Resonance Apparatus

For some reason, this demonstration never made it into the 20th century. It was designed by Felix Savart (1791–1841) to demonstrate resonance. The rim of the cup is set into oscillation by drawing a rosined violin bow across it. The sound is picked up by the resonator, provided that length of the open cylinder on the left-hand side is adjusted to be one quarter of the wavelength (plus a small end correction). Moving the resonator away from the cup will reduce the volume. This apparatus was sold by Queen of Philadelphia about 1890 for \$20.00. It was photographed in the collection of the University of Utah. (Picture and text by Thomas B. Greenslade, Jr., Kenyon College)